ADVANCED MATERIALS INTERFACES
www.advmatinterfaces.de

A Thermodynamic Description of Turbulence as a Source of Stochastic Kinetic Energy for 3D Self-Assembly

Per A. Löthman, Tijmen A. G. Hageman, Miko C. Elwenspoek, Gijs J. M. Krijnen, Massimo Mastrangeli, Andreas Manz, and Leon Abelmann**

The extent to which one can use a thermodynamic description of turbulent flow as a source of stochastic kinetic energy for 3D self-assembly of magnetically interacting macroscopic particles is investigated. It is confirmed that the speed of the objects in the flow field generated in this system obeys the Maxwell–Boltzmann distribution, and their random walk can be defined by a diffusion coefficient following from the Einstein relation. However, it is discovered that the analogy with Brownian dynamics breaks down when considering the directional components of the velocity. For the vectorial components, neither the equipartition theorem nor the Einstein relation is obeyed. Moreover, the kinetic energy estimated from the random walk of individual objects is one order of magnitude higher than the value estimated from Boltzmann statistics on the interaction between two spheres with embedded magnets. These results show that introducing stochastic kinetic energy into a self-assembly process by means of turbulent flow can to a great extent be described by standard thermodynamic theory, but anisotropies and the specific nature of the interactions need to be taken into account.

1. Introduction

Self-assembly is the autonomous organization of objects into a structure without human intervention.[1] The final properties of the assembled structure are exclusively based on the inherent properties of the individual objects.[2] Self-assembly has been achieved at different scales and in multiple ways, including evaporation-induced self-assembly,[3] ionic self-assembly,[4] self-assembly based on molecular recognition,[5,6] DNA self-assembly,[7] and colloidal crystal self-assembly.[8] The self-assembly of carbon nanotubes, graphene oxide,[9,10] and photonic crystals,[11] as well as aspects such as the influence of microgravity,[12] surfaces,[13] and supramolecular engineering,[4,14] has also been evaluated.

In all varieties of and approaches to self-assembly, three elements are common and critical: the characteristics of the individual objects, such as their mutual binding forces and geometrical shapes, the environment that may promote assembly with templates or other forms of guidance, and the disturbing forces that oppose the binding forces and thus allow the objects to explore the associated energy landscape and find a global minimum of the energy.[15]

In our earlier paper,[16] we introduced a macroscale self-assembly process using magnetic interaction between the objects and a turbulent flow as a source of disturbing forces. We discovered that the random walk of the objects in the turbulent flow can be successfully described by thermodynamic theory. In this paper, we focus on the disturbing forces, and investigate up to what point the thermodynamic description is valid. This question is highly relevant for the self-assembly of objects that are so big that thermal energy is no longer sufficient to drive the system into an energy minimum.

In self-assembly with very small objects, such as atoms or molecules, the thermal energy kT is adequate because according to the equipartition theorem it corresponds to significant random (Brownian) motion ($kT = (1/3)m\langle v^2\rangle$). However, for larger objects, roughly above 1 µm, thermal energy can no longer provide a sufficient disturbing force[2]: the objects would disintegrate rather than self-assemble. Hence, to self-assemble macro-objects, alternative ways to provide disturbing forces are used, mostly by some form of shaking.[17]

Even though shaking in the self-assembly of micrometer-sized objects has the same function as the thermal energy in the self-assembly of atoms or molecules, there are very distinct differences. In the first place, shaking is a dissipative process. When we stop shaking, the random motion of the objects comes to a halt. The energy we provide to the system is partially transferred to the objects, but at the cost of losing energy into heat along the way.

Second, shaking introduces a directionality into the disturbing forces. It is impossible to shake in all directions simultaneously. One relies on random processes, such as collisions,

P. A. Löthman, T. A. G. Hageman, A. Manz, L. Abelmann
KIST Europe
66123 Saarbrücken, Germany
E-mail: Per.Loethman@gmail.com
P. A. Löthman, T. A. G. Hageman, M. C. Elwenspoek, G. J. M. Krijnen, L. Abelmann
University of Twente
7522 NB, Enschede, The Netherlands
E-mail: l.abelmann@utwente.nl
M. Mastrangeli
Delft University of Technology
2628 CT, Delft, The Netherlands
The ORCID identification number(s) for the author(s) of this article can be found under https://doi.org/10.1002/admi.201900963.

DOI: 10.1002/admi.201900963

to randomize the direction of the forces. Since shaking is a dissipative process, the effect of randomization has a limited lifetime. Therefore, a signature of the initial direction of shaking will always be present.

Both deviations from thermal energy, i.e., dissipation and directional dependence, are present in all experiments where shaking is involved. Our macroscale setup provides an easy way to study the nature of the disturbing forces. The outcome is of general importance for the study and implementation of self-assembly.

1.1. Methods to Provide Disturbing Forces

Shaking the support on which the objects are placed is a common method to provide disturbing forces in a self-assembly system. Friction is used to transmit the energy to the object, as first shown by Penrose.[18] The adhesion force between the objects and the support varies with location, which causes a random motion.

This is used in two dimensions by placing objects on a moving platform with a linear or orbital shaker,[19–21] but also pseudorandom shaking has been applied.[22] Rather than using stiction and friction, one can place objects on smooth vibrating surfaces. This is exploited in experiments where the objects are placed at a liquid–air interface, which is disturbed by shaking the container[23–27] or by ultrasound.[28] Random motion is caused by collision with the wall of the container and between the objects themselves.

In three dimensions, objects are shaken,[29,30] or rotated[31] within containers; or one can submerge the objects and agitate the fluid to induce particle motion, for instance, by rotating[32–36] or shaking[35,37] the container, or by moving the liquid itself by ultrasonic agitation[35,38–41] or a pulsating flow.[42,43] An interesting variation on this approach is to use diamagnetic levitation and exploit the inertia of the objects to drive them out of energy minima.[44]

Instead of applying mechanical forces, one can apply disturbing energy by an external magnetic field to magnetic objects.[45,46] The magnetic field is relatively uniform around each particle; therefore, random motion relies on collisions in this case. However, when the objects are self-propelling, for instance, by the decomposition of hydrogen peroxide,[47] random motion naturally occurs.

In the aforementioned examples, the focus of the research was on the products of the self-assembly process, not on the disturbing force itself. It is tempting to compare the energy provided to the system by some way of shaking to thermal energy. For example, one can analyze the distribution of the products generated by the self-assembly process by Boltzmann statistics. Attempts have been made to introduce an "effective temperature"[19,36] or "propulsion energy."[28] In this paper, we study in more detail the nature of the disturbing forces, and to what extent they can be described by standard thermodynamic theory.

1.2. Self-Assembly as a Tool for Technology and Research

We are interested in 3D self-assembly as a manufacturing method for next-generation electronics[2] and novel materials and devices,[1,48,49] as well as in the advantages that studying self-assembly at the macroscale might bring compared to the microscale.

Scanning electron microscopy and other microscopy images often show the result of micro- or nanoscopic self-assembly, but they do not reveal the process and dynamics behind it. We cannot see how the structure formed or which pathways were taken. In situ transmission electron microscopy reveals self-assembly events rather than the entire self-assembly process itself and its underlying dynamics.[50,51] Moreover, it is impossible to avoid the influence of the electron beam on the physical and chemical properties of the particles as well as on the resolution of the footage. It is likely that a change in the properties of the particle can lead to altered particle interactions and therewith an altered self-assembly. The effects of the electron beam are even more complex when using liquid and gas environments at elevated temperatures rather than vacuum.[52]

Self-assembly often includes rapid phenomena, such as protein folding or supramolecular or nanoparticle self-assembly, which can hardly be observed directly at the microscopic level. Via macroscopic experimentation, we can overcome these obstacles by using representative particles and an analogous macroscopic self-assembly reactor, such as the one used in the research presented here. The dynamics of the self-assembly process appears much slower at the macroscopic level and can therefore be readily observed.

1.3. Macroscale 3D Self-Assembly

One aspect common to many 3D self-assembly systems is that the micro- or macroscopic particles stand or sediment onto the bottom of the vessel when there is no agitation. Self-assembly studies as a function of the strength of the disturbing forces are consequently complicated. We therefore designed a system where the function of levitating the objects is separated to a large extent from the function of disturbing the system.[16]

Levitation is achieved by introducing a flow opposite to the force of gravity, counterbalancing the drop velocity of the objects in the fluid. Agitation is achieved by intentionally introducing a turbulent flow into the system by an asymmetric fluid inflow.

As an example, **Figure 1** shows excerpts of a video recording (available in the Supporting Information) of the self-assembly of 12 polymer spheres of diameter 2 cm with embedded permanent magnets. The formation of the structure depends on the degree of turbulence: at maximum turbulence, the spheres are disconnected and start to form structures as the turbulence decreases. At low turbulence, the minimum energy structure (ring) is formed. This is a macroscopic representation of a microscopic quenching or cooling sequence and nicely demonstrates the paths of self-assembly.

In this system, we thoroughly analyzed the motion of the individual objects.[16] We have concluded that the random motion of the objects can indeed to a large extent be described by standard thermodynamic theory.

The speed of the objects obeys the Maxwell–Boltzmann distribution, and there is a well-defined diffusion constant, so that the Einstein relation $kT = fD$ is obeyed. Hence, the concept of an effective temperature has merit. However, we also found

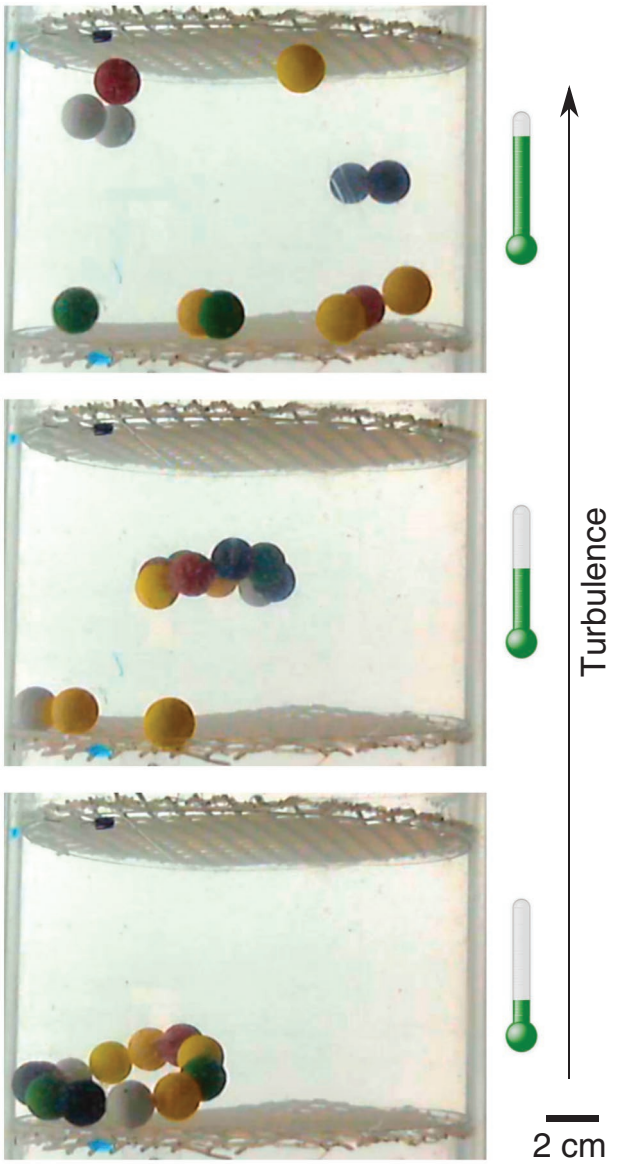

Figure 1. The effect of the degree of turbulence on the structure formation of 12 magnetic polymer spheres that self-assemble in a vertical turbulent flow. Decreasing turbulence leads to increased structure formation (lines and rings of different lengths and shapes). At maximum turbulence, only single spheres appear, whereas at minimum turbulence the lowest-energy structure (a 12-sphere ring) appears. The local magnetic forces of each individual sphere interact as the spheres explore the energy landscape in order to find the configuration of lowest energy. A video is available in the Supporting Information. (The image of the thermometer to the right of each image was adapted with permission from the version by ARTunchained.)

that there are limitations to the validity of the thermodynamic description. For instance, the speed distribution and the diffusion coefficient were not dependent on the mass of the objects. Moreover, the kinetic energy determined from the random motion was considerably higher than the energy determined from the interaction between magnetic objects using Boltzmann statistics. We suspect that the dissipative nature of turbulence lies at the origin of this discrepancy. In this paper, we present a thermodynamic description of self-assembly processes that use turbulence as source of disturbing forces. We particularly investigate the effect of the strength of the turbulence and analyze the directional components of the random motion of the objects.

2. Theory

The analysis of particle trajectories and two-particle interactions was introduced in ref. [16] Here, we also analyze the diffusion coefficient and velocity distribution for the projection of the particle movement on the vertical axis (z), i.e., along the main direction of the flow, and in the horizontal plane perpendicular to the flow (x, y). The diffusion of a particle in a confined space was described in ref. [16] for 1D movement along a line segment. If the motions of the particle along the three projections are uncorrelated, we can apply the same expression for the average squared displacement

$$< x^2 > = \sigma_x^2 \left(1 - \frac{x_t n(x_t, \sigma_x)}{N(x_t, \sigma_x) - (1/2)} \right) \quad (1)$$

where $n(x, \sigma_x)$ is the normal distribution and $N(x, \sigma_x)$ is the cumulative normal distribution. For x, we can substitute the y or z coordinate. The standard deviation of the displacement is denoted by σ_x and the variance σ_x^2 can be related to the diffusion coefficient along a coordinate in one direction by

$$\sigma_x^2 = 2D_x t \quad (2)$$

In ref. [16], we used the Maxwell–Boltzmann distribution to describe the distribution of the speed in terms of the most probable speed (or mode) v_p. The distribution of the individual components of the velocity is Gaussian with the standard deviation ϕ and zero mean velocity component

$$p(v_x) = \frac{1}{\sqrt{2\pi\phi_x^2}} \exp\left(-\frac{v_x^2}{2\phi_x^2} \right) \quad (3)$$

where again x can be substituted with y or z.

In thermodynamic theory, the disturbing forces are described in terms of the thermal energy kT. In the case of shaking, one can describe the disturbing forces in terms of an "effective" temperature,[19,36] which is much higher than the real temperature. However, the term "effective temperature" implies that all aspects of the random motion of the components can be described by standard thermodynamic theory. Therefore, we introduced the term "disturbing energy" in our earlier work.[16] As with thermal energy, this "disturbing energy" is in fact the stochastic contribution to the kinetic energy of the particles. We believe it is more accurate to use the term "stochastic kinetic energy," or simply "kinetic energy" when the context is clear. These terms will be used throughout this paper.

3. Results

We observed the movement of a single sphere and the interaction between two spheres in the reactor, and determined the

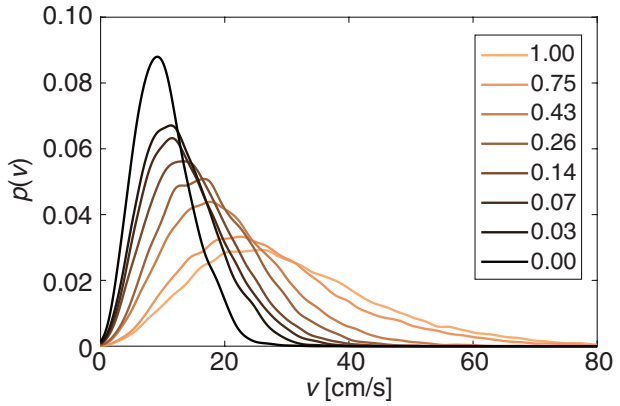

Figure 2. The distributions in the speed of a single particle for different settings of the flow asymmetry in the reactor show a Maxwell–Boltzmann-like distribution. The distribution was obtained via a kernel density estimation using a Gaussian kernel with $\sigma = 1$ cm s^{-1}. Increased turbulence leads to a higher average speed.

stochastic kinetic energy as a function of the flow asymmetry, applying the methods introduced in ref. [16]. We also investigated the directional dependency in the velocity distribution.

3.1. Relation between Flow Asymmetry and Stochastic Kinetic Energy

We observed the influence of turbulence on the kinetic behavior of a single particle in terms of the most probable speed v_p and its diffusion coefficient, as well as the interaction between two particles. From these observations, we determined the relation between the flow asymmetry and the stochastic kinetic energy.

3.1.1. Influence of Flow Asymmetry on Speed

Figure 2 shows the distribution of the speed of a particle in a turbulent flow for various settings of the flow asymmetry. These probability density functions were obtained by a kernel density estimation using a Gaussian kernel with a standard deviation of 1 cm s^{-1}. With increasing flow asymmetry, there is an increase in the speed of the particle.

The measured distribution of the speed was fitted to a Maxwell–Boltzmann distribution, as described in ref. [16], with only the most probable speed v_p as the fitting parameter. **Figure 3** shows v_p as a function of the flow asymmetry. This relation is approximately linear. Over the full range of the available flow asymmetry, the speed varies by a factor of 3 from ≈10 to 30 cm s^{-1}.

3.1.2. Influence of the Flow Asymmetry on the Diffusion Coefficient

The diffusion coefficient was estimated by fitting a confined random walk model to the measured average squared displacement.[16] The latter was obtained by averaging the squared displacements of the trajectories with a duration of 2 s. **Figure 4** shows the diffusion coefficient as a function of the asymmetry of the flow. As in the case of the speed, the diffusion increases roughly linearly with the asymmetry of the flow, now by a factor of 6 from ≈7 to 44 cm^2 s^{-1} (minimum and maximum turbulence, respectively).

3.1.3. Influence of the Asymmetry of the Flow on the Stochastic Kinetic Energy

As described in ref. [16], the speed distribution as well as the diffusion coefficient of a single sphere can be related to the stochastic kinetic energy through $kT = (1/2)m^* v_p^2$ and the Einstein relation $kT = fD$.

A third method for obtaining the stochastic kinetic energy makes use of the interaction between the particles. When

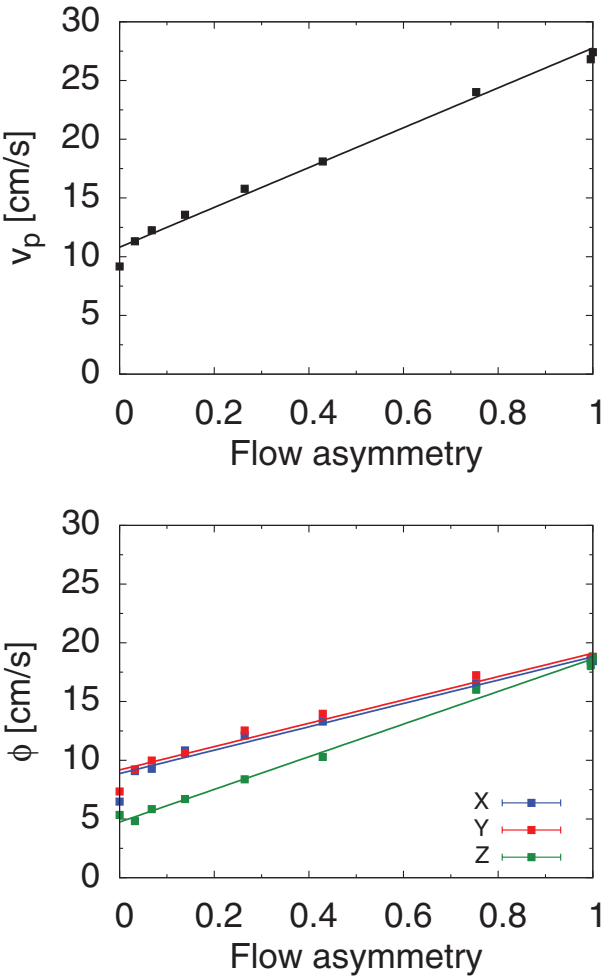

Figure 3. Top: The mode v_p of the Maxwell–Boltzmann distribution of the speed of the particle as a function of the asymmetry of the flow. The relation is approximately linear. The most probable speed (mode) increases by almost a factor of 3, indicating that the turbulence is increased. Bottom: The standard deviation of the horizontal (x, y) and vertical (z) components of the particle velocity as a function of the asymmetry of the flow. The width of the velocity distribution in the vertical direction is significantly smaller than that in the horizontal direction for a flow asymmetry below 0.5.

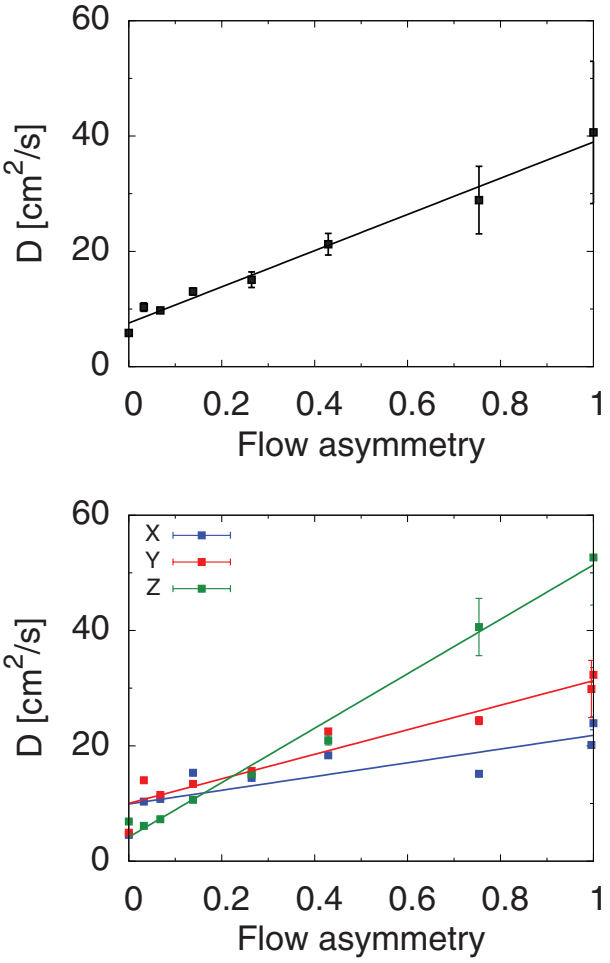

Figure 4. Top: The diffusion coefficient of the motion of a single particle as a function of the asymmetry of the flow. The relation is roughly linear. Bottom: The diffusion coefficient for each direction as a function of the asymmetry of the flow. Above an asymmetry of 0.5, the difference between the components is fairly large, but reduces significantly for lower turbulence.

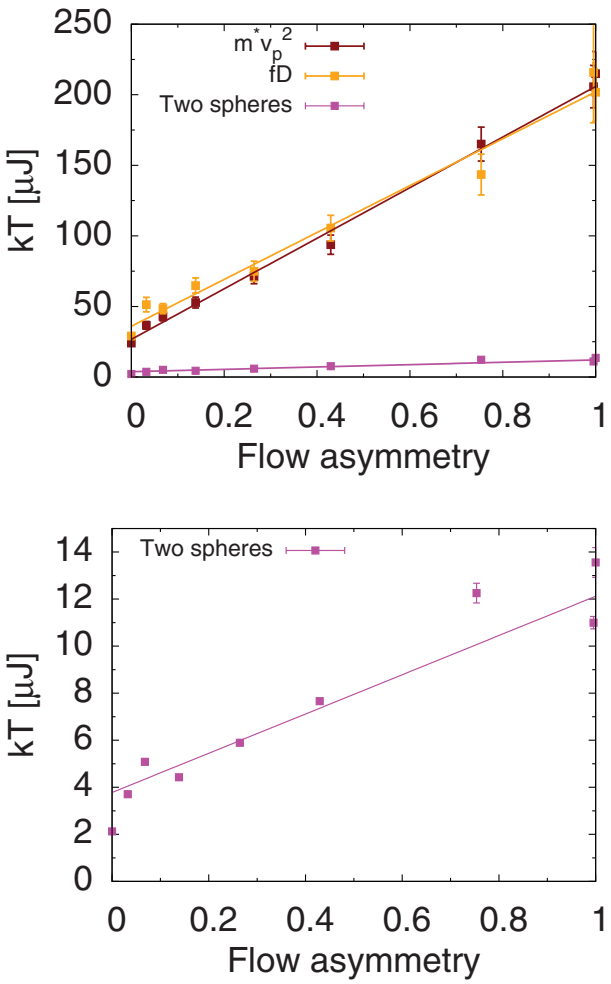

Figure 5. Stochastic kinetic energy (kT) as determined from the single-sphere experiments, using the diffusion coefficient (Einstein relation fD), using $(1/2)m^*\nu_p^2$, and using the interaction between two spheres. The kinetic energy determined from the speed distribution agrees very well with that obtained from the diffusion coefficient. However, the values obtained from the single-sphere experiments are an order of magnitude higher than those from the two-sphere experiment (enlarged at the bottom).

two particles are inserted in the reactor, they connect and disconnect intermittently. The ratio between the time they are connected and disconnected depends on their magnetic interaction energy and the kinetic energy in the system. In ref. [16], a method is described to determine this energy from the distribution of the observed particle distances. This method is more precise and fundamentally more correct than the method based on the durations of the connections and disconnections.

Figure 5 shows all estimates for the stochastic kinetic energy, plotted together. The relation between kT and the asymmetry of the flow fits well to a linear function in all three cases. The coefficients of fit are listed in **Table 1**. The estimates of the kinetic energy from the single-sphere experiments are very similar. However, like in ref. [16], these values are an order of magnitude higher than the values obtained from the two-sphere experiments. For both the single- and the two-sphere experiments, the kinetic energy increases with increasing flow asymmetry. The increase is higher by a factor of ≈2 for the single-sphere experiment (for the single-sphere experiment, the increase $a/b = 5 \pm 2$, and for the two-sphere one, $a/b = 2.1 \pm 0.07$).

The flow asymmetry is a parameter specific to our setup. To generalize the results, we analyzed the ratio between the diffusion coefficient and the speed. Equating the stochastic kinetic energy obtained from the diffusion coefficient to that obtained using the velocity, we obtain $D=(1/2)\tau_v\nu_p^2$, where $\tau_v = m^*/f$ is

Table 1. Results of linear fits ($ax + b$) of the stochastic kinetic energy to the flow asymmetry, using the kinetic energy $m^*\nu_p^2$, diffusion coefficient fD, and interaction between two spheres using Boltzmann statistics.

	Slope (a)	Offset (b)
$m^*\nu_p^2$	179 ± 9	27 ± 2
fD	166 ± 9	36 ± 5
Boltzmann	3.8 ± 0.3	8 ± 2

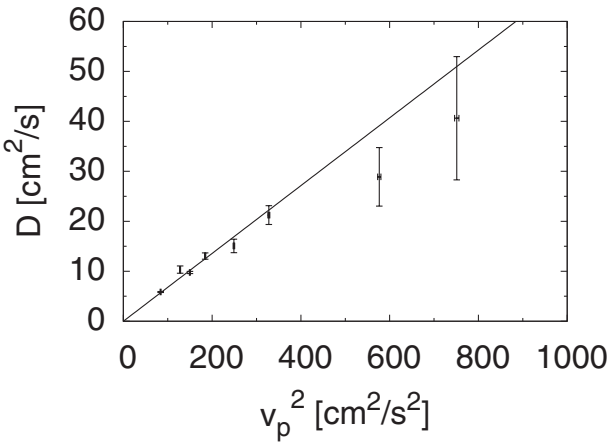

Figure 6. Diffusion coefficient versus the square of the mode of the speed distribution. The ratio is constant, with a slope of 68 ± 11 ms. This value is close to the theoretical prediction of $(1/2)\,\tau_v = 83 \pm 11$ ms.

the characteristic time separating the ballistic regime from the Brownian motion regime.[16,54] **Figure 6** shows that the plot of D versus v_p^2 is indeed approximately linear. The slope of the fit is 68 ± 1 ms, which is close to the value of $(1/2)\,\tau_v = 83 \pm 11$ ms and very similar to the value 0.1 s reported by Ilievski et al. for 1 cm blocks in a turbulent flow.[36] This result is encouraging, considering that in our analysis the effective mass m^* and effective drag coefficient f are measured independently.

3.2. Directional Dependence of Stochastic Kinetic Energy

The water flow is directed from the bottom to the top in the reactor in order to counteract the action of gravity on the particles. It is therefore expected that the vertical (z) component of the motion of the particle deviates from the horizontal (x and y) components. Additionally, there might be an asymmetry in the xy-plane as well, since the flow is injected asymmetrically at high turbulence. These effects are present in both the velocity distribution and the diffusion coefficient.

3.2.1. Directional Dependence of Velocity

Figure 7 shows the velocity distribution of a particle in a turbulent flow for various settings of flow asymmetry. Also, in this case the graphs were obtained by a kernel density estimation using a Gaussian kernel with a standard deviation of 1 cm s^{-1}. With increasing flow asymmetry, the velocity distribution becomes wider, so that the average absolute value of the velocity increases. The velocity in the horizontal directions is similar, but the vertical velocity is significantly lower for settings of low asymmetry. In accordance with theory, a normal distribution (Equation (3)) was fitted to the measurements. The standard deviation ϕ is plotted in Figure 3. There is no significant difference in the horizontal directions (x and y components), and there seems to be no correlation of the difference with the degree of asymmetry of the flow. For flow asymmetry, below 0.5, the velocity in the z-direction is significantly lower, by up to a factor of 2.

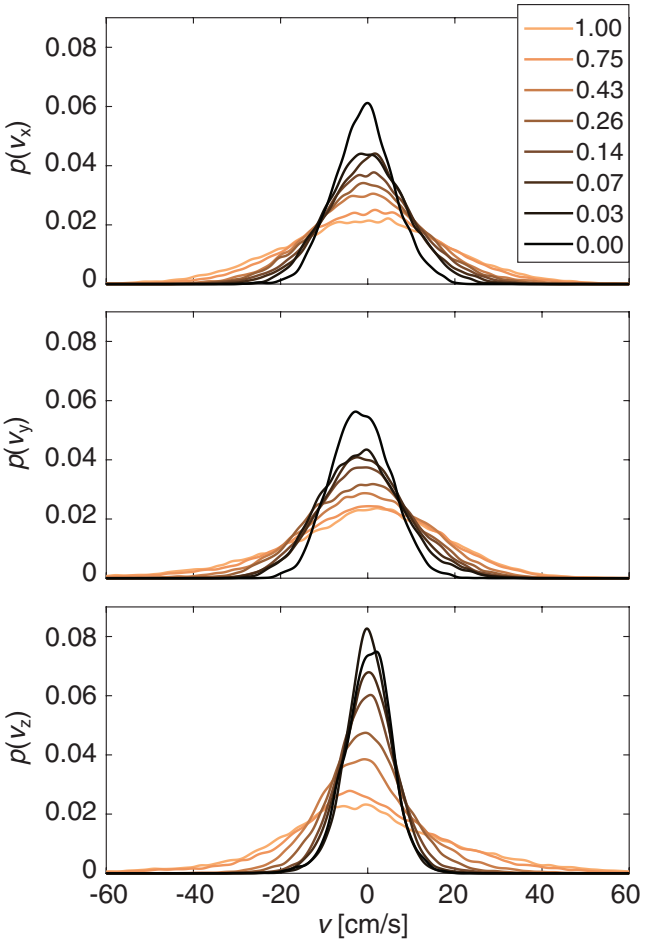

Figure 7. The x, y, and z components of the velocity of a single particle for different settings of the flow asymmetry in the reactor show a Gaussian-like distribution. The distribution was obtained via a kernel density estimation using a Gaussian kernel with $\sigma = 1$ cm s^{-1}. Increased turbulence leads to a wider velocity distribution. The z component of the velocity has a significantly lower distribution width than the horizontal components.

3.2.2. Directional Dependence of the Diffusion Coefficient

Figure 4 shows the diffusion coefficients along the three different directions. Even though the data are scattered, the values for the horizontal directions only differ moderately. The diffusion coefficient in the z-direction, however, shows a much stronger dependence on the flow asymmetry, diving below that for the horizontal components for low flow asymmetry, and vice versa.

3.2.3. Directional Dependence of Stochastic Kinetic Energy

The kinetic energy can be derived from the velocity and diffusion coefficients for the individual x-, y-, and z-components as shown in **Figure 8**. For clarity, two graphs are plotted, one for the estimate based on the kinetic energy ($kT = m^*\phi^2$, top) and one for the estimate based on the Einstein relation ($kT = fD$, bottom). Of course, these graphs show similar trends as Figures 3 and 4, as the particle mass and drag coefficient do not

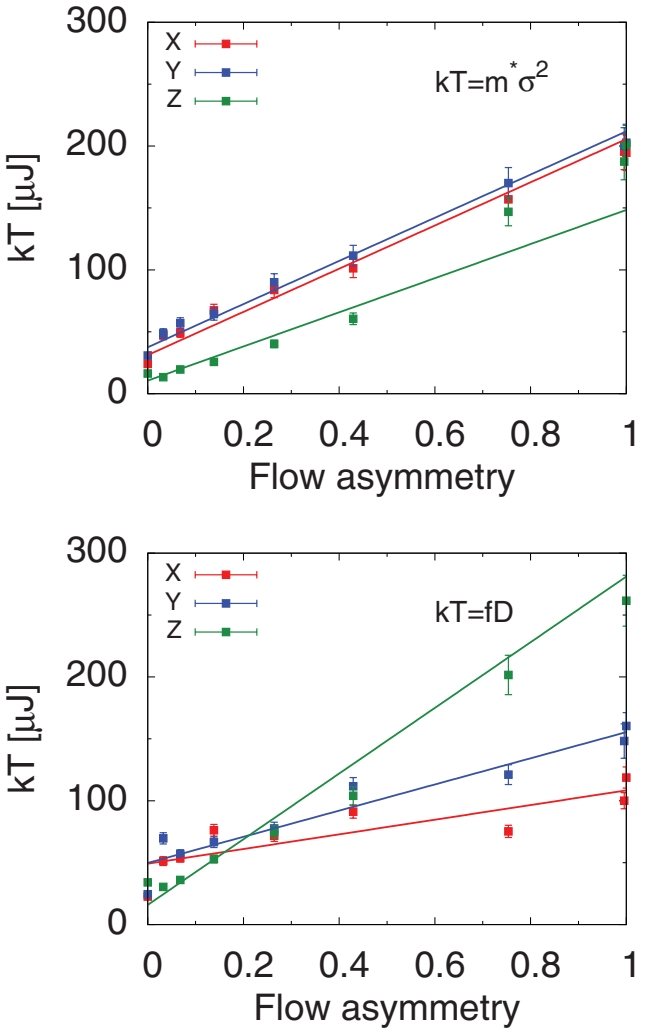

Figure 8. The stochastic kinetic energy in the three different directions, derived from the velocity (top) and from the diffusion coefficient (bottom). In general, the energy in all directions increases with increasing flow asymmetry. The estimate based on the diffusion coefficient suffers from scatter, even though the measurements themselves are precise (error bars). When considering the velocity distribution, the energies in the horizontal (*xy*) directions are equal, but twice as large as the energy in the vertical (*z*) direction for flow asymmetries below 0.5.

change between the measurements: the velocity and the diffusion coefficient fully determine the shape of these curves.

Using the velocity distribution, the stochastic kinetic energy is equal in the horizontal plane within the measurement error. However, for flow asymmetries below 0.5, the energy in the vertical direction is less than half of that in the horizontal directions. When using the diffusion coefficient to determine the directional dependence of the stochastic energy, the scatter in the estimates is higher even though the fits are still precise (error bars). The estimated values of the stochastic kinetic energy are in the same range as that of the estimates based on the velocity, especially at low flow asymmetry. The analysis suggests that an estimate based on the velocity distribution is to be preferred when considering the directional dependence, as it suffers less from scatter.

4. Discussion

Our experiments clearly show that the particle velocity, diffusion coefficient, and stochastic kinetic energy increase with the degree of turbulence. When three of the four inlet valves are gradually closed, the inflow becomes more asymmetric and the turbulence increases. This process adds to the turbulence created by the geometry of the reactor.

Creating inflow asymmetry is a practical way to change turbulence and mimic temperature changes at the micro- and nanoscale. The analogy between turbulent motion and thermal fluctuation is quite intriguing. There are, however, at least two aspects where the analogy between turbulence and thermal fluctuation does not hold: isotropy and spatial frequency power density.

4.1. Anisotropy in Turbulent Flow

The experiments show that one cannot ignore the directionality of the turbulent flow field. In analogy with temperature fluctuation, we would have to conclude that the temperature in the system is anisotropic.

Judging from the observations on the directional dependence, an increase in turbulence has a more pronounced influence on the vertical direction. The differences in the velocity, diffusion coefficient, and stochastic kinetic energy between the *x*- and *y*-directions are mild, especially compared to those of the *z*-component. The latter also has a higher range between its minimum and maximum values at the extremes of the flow asymmetry.

The anisotropy of the stochastic kinetic energy is more pronounced when derived from the Einstein relation than it is when derived from the velocity. This might have to do with the nature of the velocity: the theory of diffusion assumes a purely random process. A bias might affect how this velocity contributes to the observed displacement over time, and in this way to the validity of Equation (2).

There is a region around the flow asymmetry minima of 0.5, in which the directional dependence is a minimum. We are confident that the directional differences between the variables can be minimized by proper technical reconstruction of the self-assembly reactor. Altering the number and location of the inlet tubes and valves might be one possible option to create a more homogeneous 3D flow field in which multiparticle self-assembly can be realized.

4.2. Length Scale

The value of the stochastic kinetic energy determined via the two-particle experiments is an order of magnitude lower than that obtained from the diffusion or velocity of a single particle. We believe that this is because a greater part of the provided energy contributes rather to the motion of the single particles than to their close interaction. There is a vortex hierarchy in turbulent flow (Richardson cascade[55]). Hence, the larger vortices in a turbulent flow must first break up into smaller vortices, until viscous forces become significant and dissipate energy.

Furthermore, we assume that the asymmetrical introduction of the turbulent flow causes a macroscopic swirl with a

diameter similar to the diameter of the tank at the bottom of the cylinder. We think that the swirl moves upward in a screw-like manner and may actually represent the largest vortex in a Richardson cascade. We observed how a stream of air bubbles moved upward in a screw-like manner with a screw diameter approaching the diameter of the tank as they were introduced at the bottom of the self-assembly reactor.

Due to the Richardson cascade, there is an energy transfer from larger vortices to smaller ones. The energy is not uniformly distributed over the length scales, and drops off at shorter length scales.[56] So, in contrast to thermal fluctuation, the equipartition theorem does not hold for the energy spectrum (i.e., turbulence "noise" is not white). When we consider velocity or diffusion, we take into account all vortices, whereas for the two-sphere experiment, only vortices with length scales on the order of the sizes of the particles contribute to their separation. So, it is not surprising that the value of the stochastic kinetic energy derived from that experiment is lower.

4.3. Implication for Self-Assembly

The observed deviations from standard thermodynamics may not be specific to our experimental configuration, but may be present in all self-assembly experiments where some form of agitation other than thermal energy is used.

The directionality in stochastic kinetic energy may lead to an anisotropic growth of the assemblies, which could even be desirable. On the other hand, if the assemblies are free to rotate in the fluid, the growth may be isotropic.

However, the fact that the stochastic kinetic energy decreases with decreasing length scale can become an obstacle. If the assembly grows, the disturbing forces increase as well. This will limit the maximum size of the achievable assemblies. There are two measures one can take. In the first place, one can gradually reduce the power of the shaking over time, so that as the assembly increases in size, the disturbing force generated by the shaking action remains the same. Alternatively, one can ensure that when the assembly grows, the forces that are required to break it increase as well. In 1D assemblies, such as the lines and rings in Figure 1, this is not the case. However, in 2D and 3D self-assembly, the binding forces indeed increase with an increasing number of parts in the assembly.

5. Conclusions

We have analyzed the movement of centimeter-sized spheres in a vertically biased turbulent flow field, and compared this movement with the thermodynamic theory for Brownian motion.

We found that the speed of a single sphere in the turbulent flow obeys the Maxwell–Boltzmann distribution and its movement can be described by a confined random walk with a well-defined diffusion coefficient, identical to that of the Brownian motion of a sub-micrometer particle in a fluid.

We created an asymmetric inlet flow, which introduces an additional turbulence on top of the turbulence resulting from the high velocity of the flow and the geometry of the reactor. With increasing asymmetry, both the diffusion coefficient and the mode of the distribution of the speed increase. In analogy to the thermodynamic thermal energy term kT, we defined a stochastic kinetic energy, using either the effective mass of the sphere and the mode of the speed distribution ($(1/2)m^*v_p^2$) or the drag coefficient and diffusion coefficient (fD). These values are equal within the measurement error over the entire range of turbulence and increase from 25 to 200 μJ with increasing asymmetry in the inlet flow.

The analogy with Brownian motion breaks down when considering the vectorial components of the velocity. The water flow is upward, to compensate for the drop velocity of the spheres. As a result, at low turbulence, the vertical component of the velocity of the sphere is twice as large as that in the lateral direction. This difference disappears at higher turbulence. In contrast, the diffusion coefficient in the vertical direction is approximately equal to that of the lateral directions at low turbulence, but is higher by almost a factor of 3 at high turbulence. So, neither the equipartition theorem nor the Einstein relation is obeyed when considering the individual components.

The analogy with standard thermodynamics also breaks down when comparing the stochastic kinetic energies for different experiments. We estimated the stochastic kinetic energy from the interaction between two spheres with embedded magnets. This energy again increases with increasing turbulence, but is an order of magnitude lower than the value obtained from the single-sphere experiment (2.1 up to 13.6 μJ). For self-assembly studies, this value of the stochastic kinetic energy is more relevant.

These results show that the shaking due to a turbulent flow can, to a certain extent, be described by standard thermodynamic theory, but directional dependencies should be taken into account, and one cannot simply translate the value of the stochastic kinetic energy from one experimental configuration to another. This result is of importance for the self-assembly of objects with sizes above the micrometer range, where thermal motion is no longer effective and some form of shaking needs to be applied to drive the system into the minimum energy state.

6. Experimental Section

The self-assembly reactor was introduced in ref. [16]. The system has four inlet ports on the bottom of the cylinder. For this study, the inlet ports are equipped with valves. This allows us to inject the water flow asymmetrically and increase the turbulence. Two-way PVC ball valves (Type S6 DN40-14, 50 mm diameter, Praher Plastics Austria GmbH) were used.

Schematic front and top views of the reactor are shown in **Figure 9**. The valves can be opened between 0° (fully closed) and 90° (fully open). The maximum turbulence can be achieved by opening only one valve (right bottom image in Figure 9, the three remaining valves being opened by 0°) and the minimum turbulence by opening all valves fully (left bottom image in Figure 9, 90°). For simplicity, between these two extremes we decided to adjust the remaining three valves identically. A picture of the self-assembly reactor and the valves is shown in the Supporting Information.

To illustrate the effect of an asymmetric inflow, we inserted an air diffusor at the bottom of the reactor and used it to generate a curtain of bubbles. Since the bubbles tend to follow the flow, they can be used to image the flow pattern. **Figure 10** shows two frames of a high-speed movie of the bubble flow. The movie (available in the Supporting

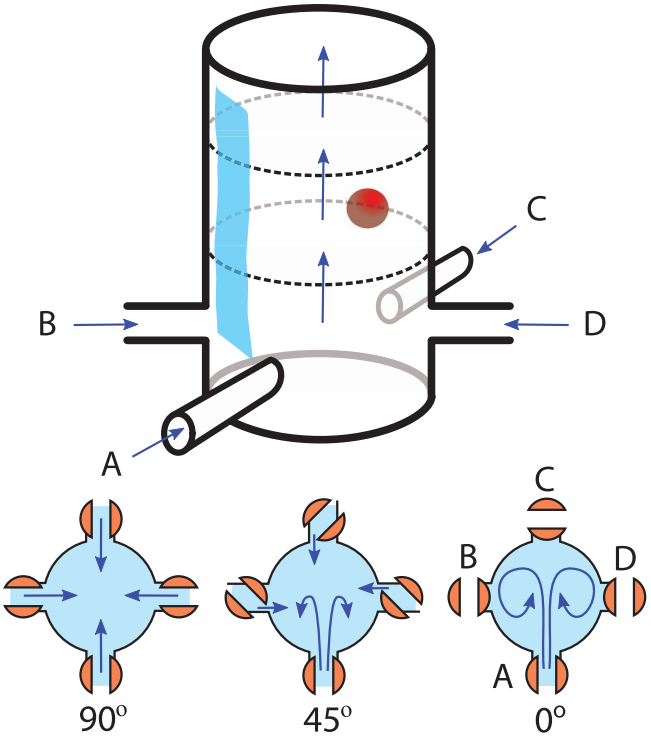

Figure 9. Top: Schematic view of the self-assembly reactor. An upward flow of water is inserted through four water inlets (A, B, C, and D). The upward flow levitates a particle (red) and provides turbulence. The dotted circles in the middle of the reactor indicate the positions of the nets that are used as placeholders for the particle(s). The turbulence in the water flow is adjusted by closing valves B, C, and D in the inlets. Bottom: Three valve settings are shown. For minimum turbulence, all valves are open (left, 90° valve opening); for maximum turbulence, valves B, C, and D are fully closed (right, 0° valve opening). A photograph of the setup and the valves is shown in the Supporting Information.

Information) was recorded at 240 fps, and is set to play back ten times slower. The flow speed of the water was 10.5 ± 0.5 cm s^{-1}.

The movie demonstrates that there is always turbulence in the reactor. This is in agreement with the speed of the flow and the diameter of the tube. We estimate the Reynolds number of the flow to be on the order of 18×10^3, which is indeed substantially above the laminar flow regime. When the flow is fully asymmetric, the turbulence increases and swirls

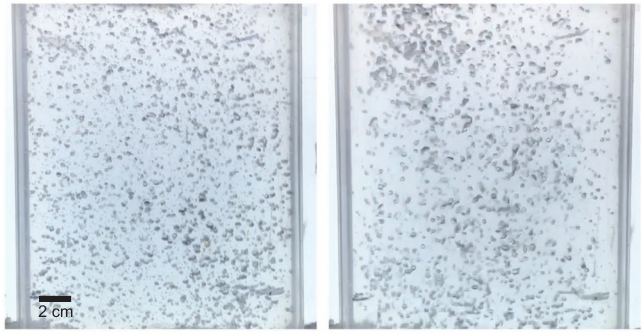

Figure 10. Bubble curtain in the upward water flow for all valves fully open (left) and three out of four closed (right). In the right image, an increase in turbulence can be observed, which is very apparent in the movie that is available in the Supporting Information.

are visible in the flow. At the experimental flow rate, it takes only around 0.5 s for the water front to travel the 18 cm from the bottom to the top of the reactor. This observation accounts for that turbulence and the vortex size distribution seem not to vary with increasing reactor height.

Flow Calibration: We expect the turbulence in the cylinder to be proportional to the asymmetry in the inflow. The inflow is determined by the angular position of the four valves. To analyze the relation between valve setting and flow, we measured the flow through the cylinder as a function of opening angle θ of one single valve (see **Figure 11**). In this measurement, the other three valves are closed and we used the maximum pump effort. We accordingly define a dimensionless measure for the asymmetry of the flow

$$\text{flow asymmetry} = 1 - \frac{f(\theta)}{f(90°)} \tag{4}$$

where $f(\theta)$ is the speed of the flow of the water through the valves controlled during the experiments, i.e., at opening angle θ. This way, at minimum turbulence, when all valves are fully open, the flow asymmetry is defined to be 0, whereas at maximum turbulence, when three valves are closed, the flow asymmetry is defined to be 1.

Particles: The particles were identical, as in ref. [16], being 18.80 ± 0.07 mm diameter ($2R$) polymer (ABS) spheres with a 3.80 × 3.80 ± 0.05 mm cylindrical NdFeB permanent magnet placed in the center of each sphere. The mass of the particles was 4.14 ± 0.01 g. In order to calculate the stochastic kinetic energy, we estimate the effective mass m^* to be 5.9 ± 0.1 g by adding 50 % of the mass of the displaced water.[16]

The terminal drop velocity v_t of the particles, measured in a column of water without flow, was 37 ± 1 cm s^{-1}, from which we estimate the drag coefficient C_d to be 0.35 ± 0.06, which is in agreement with the theoretical value of 0.39.[53] In order to estimate the stochastic kinetic energy of the particles, we introduced an effective drag coefficient[16]

$$f = \rho_{\text{fluid}} C_d \pi R^2 v_t \tag{5}$$

where ρ_{fluid} is the density of water (998 ± 3 kg m^{-3}). At this flow velocity, the value of the effective drag coefficient is 35 ± 4 g s^{-1}.

In the experiment, we set the flow velocity of the water to 18.6 ± 0.3 m s^{-1}. The flow velocity was lower than the terminal drop velocity of the sphere in order to avoid having the spheres touch the top net and get trapped there. Since during the measurement of the position the sphere is levitating in front of the camera, we employ the terminal drop velocity, rather than the flow velocity, for the estimate of the effective drag coefficient.

Reconstruction: Two synchronized cameras were used for video recordings, as described in ref. [16]. The particles were observed under different degrees of turbulence. For each setting, videos were recorded for 15 min

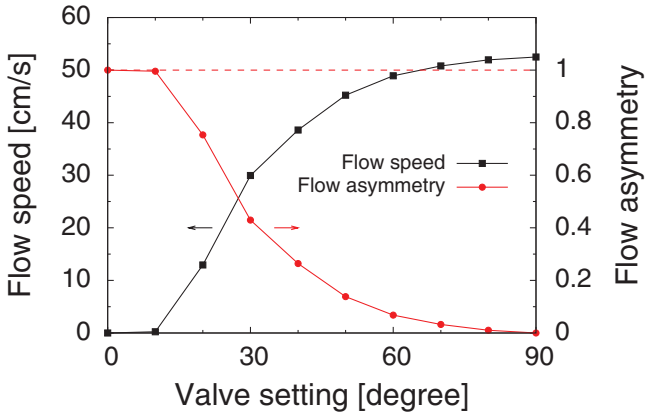

Figure 11. Flow speed through the reactor at maximum pump effort as a function of the valve angle of one valve, when the other three remain closed.

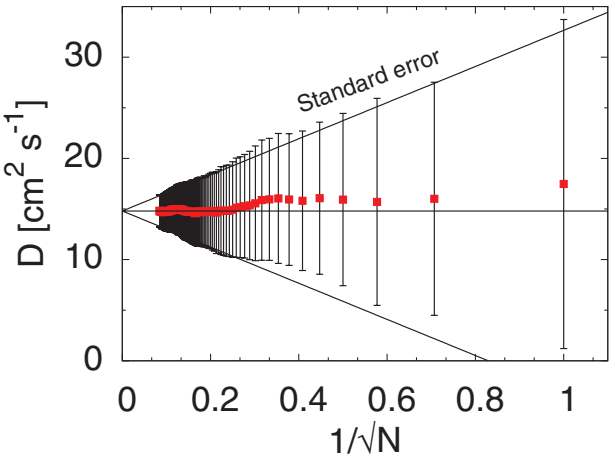

Figure 12. The estimated diffusion coefficient (red dots) and 1σ confidence interval as a function of the inverse square root of the number of trajectories (N).

for single-sphere experiments and 30 min for two-sphere experiments. Both the 3D trajectories of a single sphere and the distance between two spheres were reconstructed via custom-written MATLAB scripts.

Measurement Precision: To determine the diffusion coefficient, the trajectory of the particle in the turbulent flow was observed, as described in ref. [16]. Each trajectory longer than 0.5 s was fitted to the diffusion model described in ref. [16]. These values were averaged for a large number of trajectories to obtain an estimate of the diffusion coefficient. The precision of the estimate increases with the number of measurements, which is expressed in the standard error (the standard deviation of the fit divided by the square of the number of fits).

To validate this process, we determined the diffusion coefficient for sets of data with varying numbers of trajectories. The result is shown in **Figure 12**, where the error bars represent the estimate of the diffusion coefficient as a function of the number of trajectories N. As expected, the estimated value converges (to about 15 cm^2 s^{-1}) with increasing number of measurements. The error bars indicate the 1σ confidence limit on the estimate (we are 68 % confident that the diffusion coefficient lies between the bars). Figure 12 shows that indeed the precision of the estimate increases with the square root of the number of trajectories.

From this measurement, we conclude that for a 1σ confidence limit of 5 % of the estimated value, we need at least 570 trajectories. We obtain ≈80 trajectories of 0.5 s duration per minute. The total measurement time per experiment should therefore be at least 7 min. To be on the safe side, the duration of the experiments in this study was increased to 15 min.

Even though the estimate of the overall diffusion coefficient is well behaved, we observe a large scatter on the estimates of the diffusion coefficient of the individual components (see Figure 4). This scatter cannot be explained by the uncertainty on the estimates themselves. We conclude therefore that for the individual components, there must be other sources of uncertainty. For linear fits to the individual components (Figures 4 and 8, bottom), we therefore ignore the error estimates in the linear fits.

Supporting Information

Supporting Information is available from the Wiley Online Library or from the author.

Acknowledgements

P.A.L. and T.A.G.H contributed equally to this work. The authors would like to thank Remco Sanders for building the setup and Léon Woldering for initial work on the project. The authors further thank Michael Dirnberger for thoughtful insights, and Nikodem Bienia and Gayoung Kim for their useful contribution to the scientific work.

Conflict of Interest

The authors declare no conflict of interest.

Keywords

magnetics, self-assembly, thermodynamic, three-dimensional, turbulence

Received: May 31, 2019
Published online: July 18, 2019

[1] G. M. Whitesides, B. Grzybowski, *Science* **2002**, *295*, 2418.
[2] M. Elwenspoek, L. Abelmann, E. Berenschot, J. van Honschoten, H. Jansen, N. Tas, *J. Micromech. Microeng.* **2010**, *20*, 064001.
[3] C. J. Brinker, Y. Lu, A. Sellinger, H. Fan, *Adv. Mater.* **1999**, *11*, 579.
[4] C. F. J. Faul, M. Antoinetti, *Adv. Mater.* **2003**, *15*, 673.
[5] W. Shenton, S. A. Davis, S. Mann, *Adv. Mater.* **1999**, *11*, 449.
[6] C. Fouquey, J.-M. Lehn, A.-M. Levelut, *Adv. Mater.* **1990**, *2*, 254.
[7] Z.-G. Wang, B. Ding, *Adv. Mater.* **2013**, *25*, 3905.
[8] V. Kitaev, G. A. Ozin, *Adv. Mater.* **2003**, *15*, 75.
[9] H. Shimoda, S. J. Oh, H. Z. Geng, R. J. Walker, X. B. Zhang, L. E. McNeil, O. Zhou, *Adv. Mater.* **2002**, *14*, 899.
[10] J.-J. Shao, W. Lv, Q.-H. Yang, *Adv. Mater.* **2014**, *26*, 5586.
[11] Y. Xia, B. Gates, Z.-Y. Li, *Adv. Mater.* **2001**, *13*, 409.
[12] O. Dag, H. Ahari, N. Coombs, T. Jiang, P. P. Aroca-Ouellette, S. Petrov, I. Sokolov, A. Verma, G. Vovk, D. Young, G. A. Ozin, C. Reber, Y. Pelletier, R. L. Bedard, *Adv. Mater.* **1997**, *9*, 1133.
[13] S. Whitelam, *Adv. Mater.* **2015**, *27*, 5720.
[14] A. Ciesielski, C.-A. Palma, M. Bonini, P. Samor, *Adv. Mater.* **2010**, *22*, 3506.
[15] J. Pelesko, *Self Assembly: The Science of Things That Put Themselves Together*, Chapman & Hall/CRC Press, London **2007**.
[16] T. A. G. Hageman, P. A. Löthman, M. Dirnberger, M. Elwenspoek, A. Manz, L. Abelmann, *J. Appl. Phys.* **2018**, *123*, 024901.
[17] M. Mastrangeli, S. Abbasi, C. Varel, C. van Hoof, J. P. Celis, K. F. Böhringer, *J. Micromech. Microeng.* **2009**, *19*, 1.
[18] L. S. Penrose, R. Penrose, *Nature* **1957**, *179*, 1183.
[19] S. Tricard, C. A. Stan, E. I. Shakhnovich, G. M. Whitesides, *Soft Matter* **2013**, *9*, 4480.
[20] M. Grünwald, S. Tricard, G. M. Whitesides, P. L. Geissler, *Soft Matter* **2016**, *12*, 1517.
[21] D. Ipparthi, T. A. G. Hageman, N. Cambier, M. Sitti, M. Dorigo, L. Abelmann, M. Mastrangeli, *Phys. Rev. E* **2018**, *98*, 042137.
[22] R. Cademartiri, C. A. Stan, V. M. Tran, E. Wu, L. Friar, D. Vulis, L. W. Clark, S. Tricard, G. M. Whitesides, *Soft Matter* **2012**, *8*, 9771.
[23] B. Haghighat, M. Mastrangeli, G. Mermoud, F. Schill, A. Martinoli, *Micromachines* **2016**, *7*, 138.
[24] S. Miyashita, Z. Nagy, B. J. Nelson, R. Pfeifer, *Entropy* **2009**, *11*, 643.
[25] H. O. Jacobs, A. R. Tao, A. Schwartz, D. H. Gracias, G. M. Whitesides, *Science* **2002**, *296*, 323.
[26] N. Bowden, F. Arias, T. Deng, G. M. Whitesides, *Langmuir* **2001**, *17*, 1757.
[27] J. Tien, A. Terfort, G. M. Whitesides, *Langmuir* **1997**, *13*, 5349.
[28] S. Ahmed, D. T. Gentekos, C. A. Fink, T. E. Mallouk, *ACS Nano* **2014**, *8*, 11053.
[29] A. J. Olson, *Nat. Nanotechnol.* **2015**, *10*, 728.
[30] A. Hacohen, I. Hanniel, Y. Nikulshin, S. Wolfus, A. Abu-Horowitz, I. Bachelet, *Sci. Rep.* **2015**, *5*, 12257.

[31] K. Hosokawa, I. Shimoyama, H. Miura, *Artif. Life* **1994**, *1*, 413.
[32] A. Terfort, N. Bowden, G. M. Whitesides, *Nature* **1997**, *386*, 162.
[33] D. H. Gracias, J. Tien, T. L. Breen, C. Hsu, G. M. Whitesides, *Science* **2000**, *289*, 1170.
[34] T. D. Clark, J. Tien, D. C. Duffy, K. E. Paul, G. M. Whitesides, *J. Am. Chem. Soc.* **2001**, *123*, 7677.
[35] S. B. Shetye, I. Eskinazi, D. P. Arnold, *J. Microelectromech. Syst.* **2010**, *19*, 599.
[36] F. Ilievski, M. Mani, G. M. Whitesides, M. P. Brenner, *Phys. Rev. E: Stat., Nonlinear, Soft Matter Phys.* **2011**, *83*, 017301.
[37] H. Onoe, K. Matsumoto, I. Shimoyama, *Small* **2007**, *3*, 1383.
[38] J. C. Love, A. R. Urbach, M. G. Prentiss, G. M. Whitesides, *J. Am. Chem. Soc.* **2003**, *125*, 12696.
[39] M. Mastrangeli, A. Martinoli, J. Brugger, *Microelectron. Eng.* **2014**, *124*, 1.
[40] F. Ilievski, K. A. Mirica, A. K. Ellerbee, G. M. Whitesides, *Soft Matter* **2011**, *7*, 9113.
[41] L. A. Woldering, A. J. Been, L. Alink, L. Abelmann, *Phys. Status Solidi RRL* **2016**, *10*, 176.
[42] W. Zheng, H. O. Jacobs, *Adv. Funct. Mater.* **2005**, *15*, 732.
[43] J. Goldowsky, M. Mastrangeli, L. Jacot-Descombes, M. R. Gullo, G. Mermoud, J. Brugger, A. Martinoli, B. J. Nelson, H. F. Knapp, *J. Micromech. Microeng.* **2013**, *23*, 125026.
[44] A. Tkachenko, J. J.-Q. Lu, *J. Magn. Magn. Mater.* **2015**, *385*, 286.
[45] K. Hosokawa, I. Shimoyama, H. Miura, *Sens. Actuators, A* **1996**, *57*, 117.
[46] B. A. Grzybowski, H. A. Stone, G. M. Whitesides, *Proc. Natl. Acad. Sci. USA* **2002**, *99*, 4147.
[47] R. F. Ismagilov, A. Schwartz, N. Bowden, G. M. Whitesides, *Angew. Chem., Int. Ed.* **2002**, *41*, 652.
[48] G. M. Whitesides, J. K. Kriebel, B. T. Mayers, *Nanoscale Assembly*, Springer, Boston, MA **2005**.
[49] S. Chidambaram, K. Nehru, M. Sivamukar, *Nanostructure, Nanosystems, and Nanostructured Materials: Theory, Production and Development*, Apple Academic Press, Palm Bay, FL **2014**, pp. 437–461.
[50] Y. Liu, X.-M. Lin, Y. Sun, T. Rajh, *J. Am. Chem.* **2013**, *135*, 3764.
[51] E. Nakamura, *Acc. Chem. Res.* **2017**, *50*, 1281.
[52] M. L. Taheri, E. A. Stach, I. Arslan, P. A. Crozier, B. C. Kabius, T. LaGrange, A. M. Minor, S. Takeda, M. Tanase, J. B. Wagner, R. Sharma, *Ultramicroscopy* **2016**, *170*, 86.
[53] P. P. Brown, D. F. Lawler, *J. Environ. Eng.* **2003**, *129*, 222.
[54] X. Bian, C. Kim, G. E. Karniadakis, *Soft Matter* **2016**, *12*, 6331.
[55] L. F. Richardson, *Proc. R. Soc. Lond. A* **1926**, *110*, 709.
[56] H. Y. Hwang, G. A. Irons, *Metall. Mater. Trans. B* **2012**, *43*, 302.

